mater.scichina.com link.springer.com

Sci China Mater 2025, 68(1): 253–260
https://doi.org/10.1007/s40843-024-3148-9

Enhanced long-lasting luminescence nanorods for ultrasensitive detection of SARS-CoV-2 N protein

Yi Wei[1,2], Menglin Song[1,3], Lihua Li[1], Yingjin Ma[1], Xinyue Lao[1], Yuan Liu[1], Guogang Li[2] and Jianhua Hao[1*]

ABSTRACT **Persistent luminescence nanomaterials can remain luminescence when the light source is turned off, which exhibits promise in biosensor and bioimaging fields since they have the ability to completely eradicate tissue autofluorescence. Although significant progress has been made in the persistent luminescence biosensing, there is still a dearth of long-afterglow detection platform with low limit of detection (LOD) and high sensitivity. Herein, Zn_2GeO_4:Mn, Cr persistently luminescent nanorods (PLNRs) with superior persistent luminescence and long afterglow time were developed. The addition of Cr^{3+} manifestly improves persistent luminescence intensity and afterglow duration through creating a deep defect trap. Then the biosensors were constructed by combining the Zn_2GeO_4:Mn,Cr PLNRs-antibody and Fe_3O_4 magnetic nanoparticles (MNPs)-antibody for nucleocapsid protein detection based on electrostatic attraction. The LOD value for nucleocapsid protein realizes as low as 39.82 ag/mL, which is much lower than the previously reported persistent luminescent-based biosensors. Accordingly, the low detection sensitivity is attributed to fluorescence resonance energy transfer. In addition, high specificity is also achieved. Therefore, the as-prepared Zn_2GeO_4:Mn,Cr persistently luminescent materials can act as the promising candidate in biosensors applications. This strategy provides effective guidance for the development of biosensing platforms with high sensitivity and specificity.**

Keywords: Zn_2GeO_4:Mn, Cr, persistent luminescence, biosensor, nucleocapsid protein, high sensitivity

INTRODUCTION

Biomedical diagnosis and treatment techniques play vitally important role in early diagnosis treatment and prediction, evaluation and healthcare fields [1–4]. Biosensors have been applied in the detections of cancer, virus, bacteria and so on [5–8]. One of the underlying challenges of biosensors is the lack of effective point-of-care detection approaches. Thus, the rapid-speed and definitive detection approach is important for biosensor applications. The usual detection methods include computed tomography (CT), viral culture, reverse transcription-polymerase chain reaction (RT-PCR) and enzyme-linked immunosorbent assay (ELISA) [9–12]. CT scan involves multiple X-ray scans of the patient's body at different angles to produce cross sectional images, which belongs to a non-invasive tool [13]. The disadvantage of CT for virus detection is the low specificity, detection sensitivity and accuracy [14,15]. RT-PCR is a standard technique for virus diagnostic, but it requires tedious sample pretreatment, highly trained operation staff, costly instruments and prolonged processing time [16,17]. ELISA is a rapid detection method that is established by a solid-phase enzyme immunoassay, but the relatively low sensitivity and the need for high-quality sample preparation limit its applications [18]. Hence, the development of new detection methods is a crucial issue in the further study.

Fluorescence analysis technique has been considered as one of the most powerful approaches in biosensor applications [19,20]. Fluorescence probe is the indispensable component in fluorescence analysis technique. Commonly, fluorescence probes contain organic dyes, quantum dots, and up-conversion nanoparticles (UCNPs) [21–30]. Nevertheless, the above fluorescence probes cannot completely avoid the background fluorescence signals.

Persistently luminescent material is known as "a legendary luminous pearl", exhibiting bright luminescence for few seconds to several days when stopping excitation light sources. The persistent luminescence is mainly caused by the stored excitation energy in trap energy levels [31]. Persistent luminescence performance can efficiently achieve autofluorescence-free, leading to the improvement of detection accuracy in biosensor applications [32,33]. To date, some persistently luminescent materials have been reported with excellent persistent luminescence intensity and long-lasting persistent time, like green $SrAl_2O_4$:Eu^{2+}, Dy^{3+} (>30 h), blue $CaAl_2O_4$:Eu^{2+}, Nd^{3+} (>10 h), Near infrared (NIR)-emitting $Zn_3Ga_2Ge_2O_{10}$:Cr^{3+} (>10 h) and red Y_2O_2S:Eu^{3+}, Mg^{2+}, Ti^{4+} (>5 h) [34–37]. In order to achieve potential applications in biosensors, the particles size and shape of the persistently luminescent materials were further optimized by tuning the synthesis approaches. For instance, Zn_2GeO_4:Mn^{2+} (ZGO:Mn) persistently luminescent nanorods (PLNRs) were prepared with green emission based on hydrothermal method [38,39]. $ZnGa_2O_4$:Cr^{3+} nanospheres with NIR persistent luminescence were successfully obtained through hot injection methods [40,41]. Previously, the persistent nanomaterials were reported to achieve potential applications in disease biomarker detection, such as SARS-CoV-2 and bacteria [42–44]. Although significant progress has been made in particle size and shape of persistently luminescence materials, the persistent luminescence

[1] Department of Applied Physics, The Hong Kong Polytechnic University, Kowloon 999077, Hong Kong, China
[2] Faculty of Materials Science and Chemistry, China University of Geosciences, Wuhan 430074, China
[3] Department of Gastrointestinal Surgery, The Third Affiliated Hospital of Sun Yat-sen University, Guangzhou 510630, China
* Corresponding author (email: jh.hao@polyu.edu.hk)

intensity and afterglow time still require further optimization. The underlying relationship between persistent luminescence and localized structure is unclear. Besides, the detection sensitivity of biosensor based on persistently luminescent materials should be further improved.

In this manuscript, we design ions co-doping strategy by introducing Cr^{3+} in ZGO:Mn PLNRs, achieving improved persistent luminescence and longer afterglow time. The underlying luminescence enhancement mechanism is attributed to the introduction of deep defect trap. The biosensors was constructed by combining the Zn_2GeO_4:Mn,Cr PLNRs-antibody and Fe_3O_4 magnetic nanoparticles (MNPs)-antibody for nucleocapsid protein (N protein) detection based on electrostatic attraction, realizing low detection of limit (LOD) of 39.82 ag/mL. The proposed strategy can provide guidance for the development of highly sensitive and specific biosensor devices.

EXPERIMENTAL SECTION

Materials

$Zn(NO_3)_2{\cdot}6H_2O$, $Cr(NO_3)_3{\cdot}9H_2O$, HNO_3 (68%), and ammonium hydroxide (28%) were purchased from Sinopharm group. $MnCl_2{\cdot}4H_2O$, GeO_2, (3-aminopropyl)triethoxysilane (APTES), *N*,*N*-dimethylformamide (DMF), and 2-(*N*-morpholino) ethanesulphonic acid (MES) were purchased from Aladdin. NaOH was purchased from Macklin. 1-(3-Dimethylaminopropyl)-3-ethylcarbodiimide hydrochloride (EDC, >98%), *N*-hydroxysuccinimide (NHS, >98%), and Fe_3O_4-SiO_2-COOH magnetic nanoparticles (MNPs) were purchased from TCI. N protein, antibody1 and antibody2, bovine serum albumin (BSA), and human serum albumin (HSA) were purchased from Beyotime Biotechnology. All chemicals were used as received without further purification.

Preparation of ZGO:Mn and Zn_2GeO_4:Mn,Cr PLNRs

ZGO:Mn and Zn_2GeO_4:Mn,Cr were prepared by a hydrothermal method, which was the same with the reported reference [38]. Firstly, 2 mol/L $Zn(NO_3)_2$, 0.5 mol/L $MnCl_2$, 0.1 mol/L $Cr(NO_3)_3$, and 1 mol Na_2GeO_3 solutions were pre-formed. In detail, $Zn(NO_3)_2$ solution was prepared by 5.9502 g $Zn(NO_3)_2{\cdot}6H_2O$ with 10 mL deionized water, $MnCl_2$ solution was prepared by completely dissolving 0.9895 g $MnCl_2{\cdot}4H_2O$ into 10 mL deionized water, $Cr(NO_3)_3$ solution was prepared by totally dissolving 0.200 g $Cr(NO_3)_3{\cdot}9H_2O$ with 5 mL deionized water, and Na_2GeO_3 solution was prepared by dissolving 1.0464 g GeO_2, and 0.7994 g NaOH into 10 mL deionized water. Secondly, 1 mL $Zn(NO_3)_2$, 500 μL HNO_3, 10 μL $MnCl_2$, and 50 μL $Cr(NO_3)_3$ were added into 20 mL H_2O with vigorous stirring. Then 1 mL Na_2GeO_3 was dropwise added into the above solution, companied with an immediate generation of white precipitate. Next, 1 mL ammonium hydroxide was slowly added into the above to adjust the pH value of 9–10. Finally, the mixture was transferred to a Teflon-lined autoclave and reacted at 200°C for 10 h in oven. The obtained ZGO:Mn and Zn_2GeO_4:Mn,Cr samples were collected after centrifugation and washed with deionized water.

Surface functionalization of Zn_2GeO_4:Mn,Cr PLNRs

Zn_2GeO_4:Mn,Cr sample was first functionalized with amino grounds (PLNRs-NH_2). 0.2 g Zn_2GeO_4:Mn,Cr PLNRs was uniformly dispersed in 8 mL DMF, and then 1 mL APTES was dropwise added into the above reaction under thoroughly stirring. The above solution was constantly stirring at 80°C for at least 12 h. The resultant solution was then washed with DMF for two times to totally remove the extra APTES. After that, the PLNRs-NH_2 was dispersed in 8 mL DMF again, 0.2 g succinic anhydride was slowly added, and the resultant solution was vigorous stirring at 60°C for 24 h. After sufficient reaction, the product (Zn_2GeO_4:Mn,Cr PLNRs-COOH) was washed with water/ethanol mixture (1:1) for 2 times, and finally dispersed in 1 mL deionized water.

Functionalization of Zn_2GeO_4:Mn,Cr PLNPs-COOH and Fe_3O_4 MNPs with antibody

Briefly, 500 μL EDC (100 mg/mL) and 750 μL NHS (100 mg/mL) were dropwise added into 500 μL Zn_2GeO_4:Mn,Cr PLNRs-COOH solution (0.5 mol/L) with adequately stirring for 30 min at room temperature. Meanwhile, 25 μL EDC (100 mg/mL) and 37.5 μL NHS (100 mg/mL) were added in 500 μL Fe_3O_4 MNPs (5 mg/mL) under stirring for 30 min at room temperature. Then, the above two solution were centrifuged. Next, the two precipitates were dispersed into 500 μL MES solution (pH = 5), respectively. 49.71 mg antibody 1 and 63.41 mg antibody 2 were added into PLNRs and MNPs solutions with incubation for 15 h, respectively. The resultant products were washed with deionized water, and then 2% BSA was added for blocking 30 min. At last, the centrifuged products were dispersed in deionized water.

RESULTS AND DISCUSSION

ZGO:Mn PLNRs was the popular candidate in biosensor and bioimaging fields due to the uniform morphology and bright green light emission and afterglow. In order to further improve the photoluminescence and persistent luminescence, ion co-doping strategy was designed. Cr^{3+} was co-doped in ZGO:Mn PLNRs. Fig. 1a shows the absorption spectra of ZGO:Mn and ZGO:Mn,Cr PLNRs, with strong absorption in the region of 200–350 nm. Obviously, the absorption intensity of ZGO:Mn,Cr is much higher than that of ZGO:Mn, indicating that the ionic co-doping strategy can remarkably improve the absorption intensity in near-ultraviolet (n-UV) region. Under n-UV light excitation, both samples exhibit broad-band green light at 534 nm that is ascribed to $^4T_1 \rightarrow {}^6A_2$ electron transition of Mn^{2+} (Fig. 1b). It is noted that the spectral shape and position keep unanimous with and without Cr^{3+}. Fig. 1c shows the persistent luminescence spectra after the removal of 360 nm laser. It is observed that the co-doping of Cr^{3+} can largely enhance the persistent luminescence intensity of about 40 folds without any spectral shape and position changes. In addition, the shape and position of persistent luminescence is consistent with that of photoluminescence.

Fig. 1d presents the persistent luminescence decay curves of ZGO:Mn and ZGO:Mn,Cr. The intensity of both samples exhibits sharply decreasing tendency at the first dozens of seconds then presents a slowly decreasing trend. Significantly, a favorably slower decay is observed with the co-doping of Cr^{3+} ions, of which the decay time to 0.1% of the initial intensity equals to 80 and 13 s for ZGO:Mn,Cr and ZGO:Mn, respectively. The above result describes that the co-doping of Cr^{3+} can remarkably improve the persistent luminescence intensity and afterglow time. The design proposal of ion co-doping strategy is also widely applied to enhance the luminescence performance in

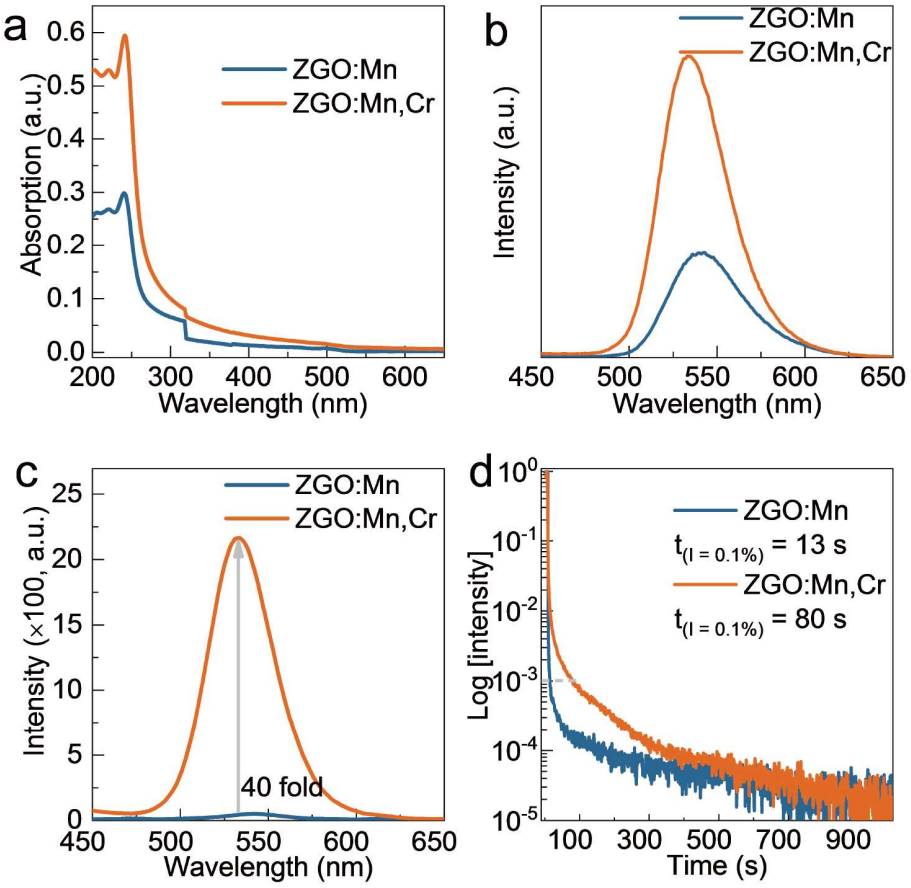

Figure 1 (a) Absorption spectra, (b) photoluminescence spectra, (c) persistent luminescence spectra and (d) normalized persistent luminescence decay curves of ZGO:Mn and ZGO:Mn,Cr PLNRs.

ZGO:Mn PLNRs materials, the corresponding enhancement mechanism is similar [45–47].

In order to clarify the underlying mechanism of the improved persistent luminescence intensity and afterglow time, we speculate the following schematic mechanism diagram (Fig. 2a, b). Due to the similar ionic radius, Mn^{2+} substitutes in Zn^{2+} sites, while Cr^{3+} prefers to occupy Ge^{4+} sites. Owing to the heterovalent substitution between Cr^{3+} and Ge^{4+}, some extra negative charge would be generated to maintain electroneutrality [48]. Therefore, the formed electron trap plays vital role in enhancing persistent luminescence and afterglow time.

Fig. 2c presents the representative X-ray diffraction (XRD) patterns of ZGO:Mn,*x*Cr ($0.5\% \leqslant x \leqslant 4\%$) PLNRs. All the diffraction peaks match well with the standard Zn_2GeO_4 (ICSD No. 68382), indicating that all ZGO:Mn,*x*Cr ($0.5\% \leqslant x \leqslant 4\%$) PLNRs materials crystallized in pure phases. As exhibited in Fig. 2d, the photoluminescence excitation spectrum of ZGO:Mn,Cr contains a broad band ranging from 250–400 nm with the maximum at 310 nm, which is in good line with the absorption spectra results. Fig. 2e presents the persistent luminescence spectra of ZGO host and ZGO:Mn,*x*Cr ($0.5\% \leqslant x \leqslant 4\%$) PLNRs when pre-irradiating with 360-nm laser for 3 min. It is noted that the persistent luminescence spectrum of ZGO host is composed of a weak broad emission band with the peak at 475 nm, further providing an evidence that the bright green persistence is ascribed to the electron transition of Mn^{2+}. In addition, when increasing Cr^{3+} doping concentration, the peak position and shape of persistent luminescence maintain consistent, indicating that the doping concentration of Cr^{3+} cannot affect the persistent luminescence behavior. With increasing the Cr^{3+} concentration from 0.5% to 4%, the persistent intensity first increases to the maximum at 2%, then decreases beyond 2%. The varied persistent luminescence intensity is caused by the trap depth modulation through increasing Cr^{3+} doping concentration. In order to analyze the persistence luminescence stability and repeatability, the photoluminescence emission and persistent luminescence spectra of ZGO:Mn,2%Cr PLNRs samples were measured for 20 times (Fig. S1). The peak position errors of both photoluminescence emission and persistent luminescence spectra are 0.3%, indicating that the green light and persistent luminescence are relatively stable.

According to the superior persistent luminescence property, mild synthesis condition, and excellent luminescence/structure stability, ZGO:Mn,Cr were employed for autofluorescence-free biosensing. Since N protein is characterized by high expression and is more prone to mutation, N protein is chosen as the detection target, and the detection methods is based on highly specific antigen-antibody response. The design and scheme of the detection is illustrated in Fig. 3. The ZGO:Mn,Cr PLNRs were functionalized with antibody 1, while Fe_3O_4 MNPs were functionalized with antibody 2. Through incubation and magnetic separation process, the suspension can be divided into two parts. Owing to the antigen-antibody reaction, the sandwich-based immunoluminescence structure including ZGO:Mn,Cr, N

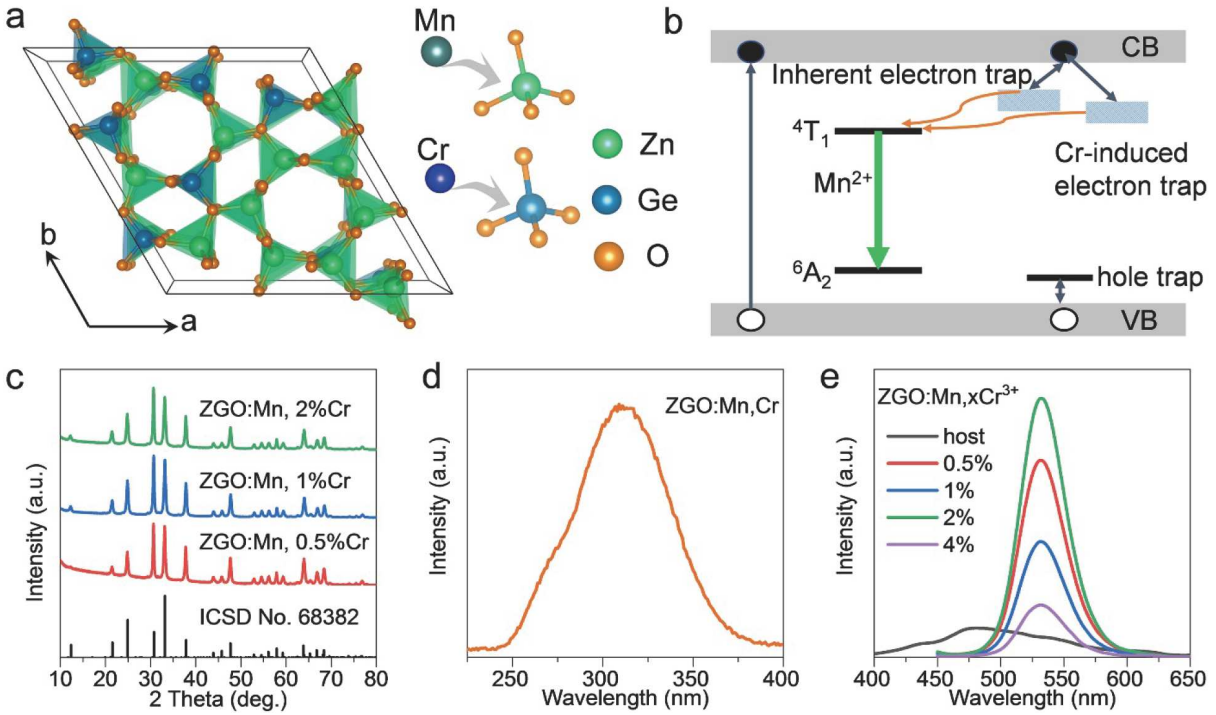

Figure 2 (a) Schematic crystal structure diagram of ZGO host and the sites occupation of Mn, Cr in ZGO. (b) Schematic persistent luminescence enhancement mechanism. (c) XRD patterns of ZGO:Mn,*x*Cr ($0.5\% \leqslant x \leqslant 4\%$) PLNRs. (d) Photoluminescence excitation spectra of ZGO:Mn,Cr sample. (e) Persistent luminescence spectra of ZGO host and ZGO:Mn,*x*Cr PLNRs ($0.5\% \leqslant x \leqslant 2\%$).

protein and Fe_3O_4 MNPs were concentrated (named as solution II). The extra ZGO:Mn,Cr would disperse in suspensions (named as solution I). The photoluminescence and persistent intensity of solution I and II should vary with the change of N protein concentration. As a result, the high-sensitive and specific detection for N protein were achieved.

Fig. 4a exhibits the transmission electron microscope (TEM) image of ZGO:Mn,Cr PLNRs. All particles crystallize in nanorod morphology with the size of around 13.4 nm × 39.2 nm. The high-resolute TEM (HRTEM) image shows clear lattice fringe, of which the interplanar spacing is calculated to 0.71 nm, in good accordance with (110) lattice plane. The above TEM result matches well with the XRD data, which provides an efficient evidence for the successful preparation of ZGO:Mn,Cr PLNRs. Fig. S2a presents the single-particle morphology of the commercially purchased Fe_3O_4@SiO_2 MNPs, which exhibits regular sphere with diameter of 700 and 30 nm SiO_2 coating layer. Before ZGO:Mn,Cr PLNRs were functionalized with antibody1, the PLNRs materials were successively treated with amidogen and carboxyl. Fig. 4c presents the zeta potential value during the functionalized antigen-antibody reaction process. The as-prepared ZGO:Mn,Cr PLNRs exhibit slightly negative potential value of −1.54 mV, and then increase to 3.45 mV in PLNRs-NH_2. When the functional group was treated with carboxyl, the zeta potential value of PLNRs-COOH decreases to −17.87 mV. Finally, the PLNRs-antibody1 shows the lowest value of −20.63 mV. The abovementioned consequence confirms that PLNRs are successfully functionalized in each step. In addition, the zeta potentials of Fe_3O_4 MNPs-antibody2 and N protein are −8.48 and 4.11 mV, respectively. This result demonstrates that the sandwich-based immunocomplexes can be stable owing to the electrostatic attraction.

Fig. 4d presents the successful formation of sandwich-based immunocomplexes based on the highly specific antigen-antibody reaction between N protein and the corresponding antibodies. In order to clarify the practical detection ability of N protein, we analyzed the morphology of control samples that is composed of PLNRs-antibody1, Fe_3O_4 MNPs-antobody2 and deionized water. Fig. S2b exhibits that PLNRs-antibody1 and Fe_3O_4 MNPs-antobody2 are dispersive without any connection. As exhibited in Fig. 4e, only ZGO:Mn,Cr PLNRs can be observed. The above consequence demonstrates that the proposal of the N protein detection is feasible. Although there is a negligible decrease in both photoluminescence emission and persistent luminescence intensity when the PLNRs sample was functionalized with carboxyl and antibody, the spectral shape and position maintained consistent. Fig. 4f presents the photoluminescence decay curves of ZGO:Mn,Cr before and after N protein detection. Both decay curves can be well fitted with bi-exponential model with the calculated average lifetime of 0.44 and 0.42 ms, respectively. The above result indicates that the green light before and after N protein detection belongs to characteristic Mn^{2+} emission.

Fig. 5a, b and Fig. S3 exhibit the photoluminescence emission and persistent luminescence spectra. The autofluorescence from 400–475 nm is remarkable in photoluminescence emission spectra when ZGO:Mn,Cr PLNRs sample were functionalized with carboxyl or antibody1, which can seriously affect the detection accuracy of N protein. Notably, no autofluorescence was observed on persistent luminescence spectra, which only contain one green emission band. In conclusion, the N protein detection based on persistent luminescence spectra can efficiently realize autofluorescence-free luminescence, further increasing the detection accuracy and sensitivity. The response

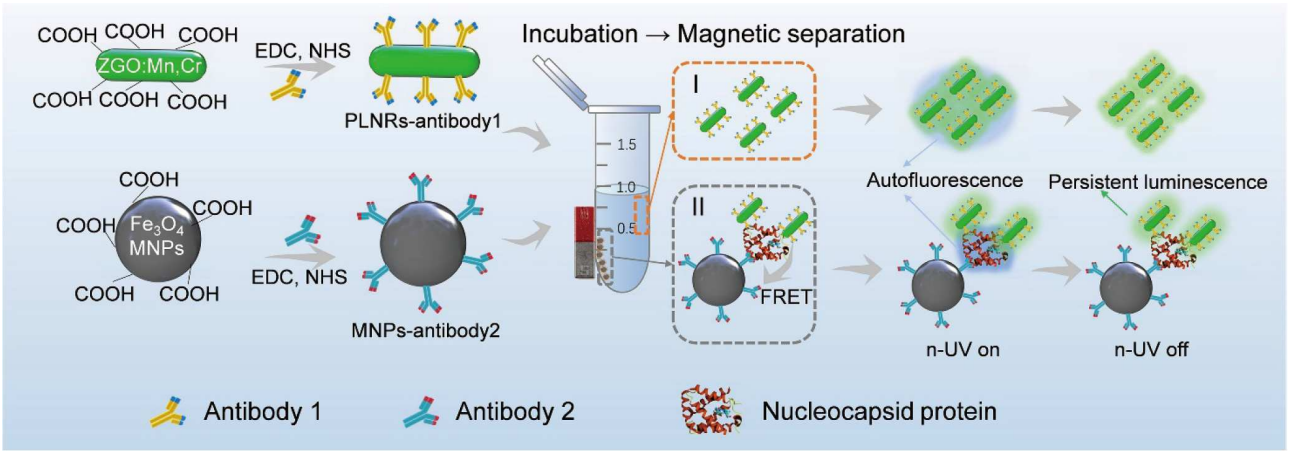

Figure 3 Schematic illustration of N protein detection by using ZGO:Mn,Cr PLNRs and Fe_3O_4 MNPs sandwich-based immunoluminescence assay.

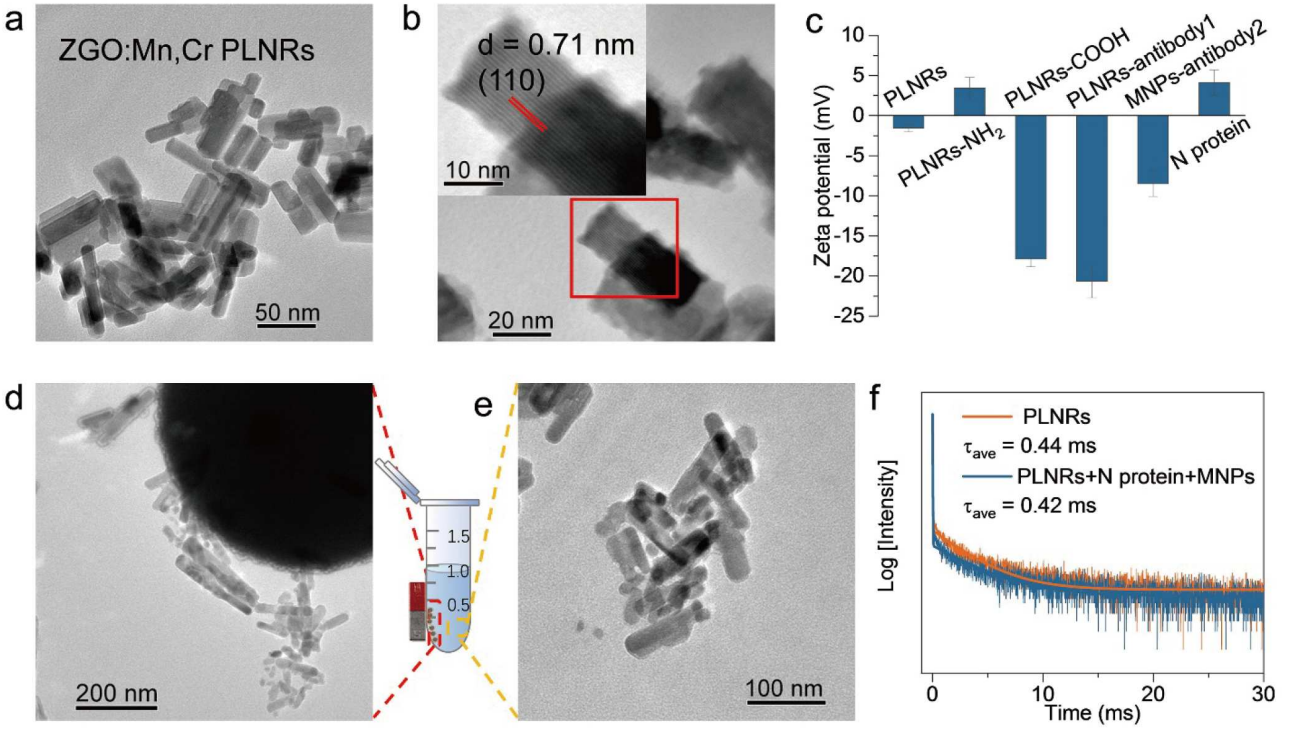

Figure 4 (a) TEM and (b) HRTEM images of ZGO:Mn,Cr PLNRs. (c) Zeta potential values of bare and functionalized nanoparticles and N protein. TEM images of sandwich-based immunocomplexes in (d) solution II and (e) solution I. (f) Photoluminescence decay curves of ZGO:Mn,Cr PLNRs and ZGO:Mn,Cr PLNRs with N protein defection based on ZGO:Mn,Cr PLNRs and Fe_3O_4 MNPs immunoluminescence (λ_{ex} = 300 nm, λ_{em} = 535 nm).

of the N protein detection was further tested. Firstly, the incubation time was analyzed, of which the N protein concentration was fixed at 1.56 fg/mL (Fig. S4). When ZGO:Mn,Cr PLNRs-antibody1, Fe_3O_4 MNPs-antibody2 and N protein were incubated for 3 min, the persistent luminescence was remarkably decrease with quenching efficiency (QE) of about 51.8%. With the increase of incubation time, the QE value slightly increases to 75.1% at 60 min. The QE value is calculated with the following equation:

$$\mathrm{QE}(\%) = \frac{I_{\mathrm{control}} - I}{I_{\mathrm{control}}} \times 100\%, \quad (1)$$

where I_{control} represents the persistent luminescence intensity of control sample without N protein, I is the persistent luminescence intensity with varied N protein concentration. As shown in Fig. 5c, the persistent luminescence intensity gradually decreases with increasing N protein concentration. As anticipated, the QE value gradually increases from 20.7% to 70.2% with increasing N protein concentration from 31.2 to 3120 ag/mL. This result indicates that the excellent detection sensitivity for N protein. As shown in Fig. 5e, a good linear relationship between persistent luminescence quenching and the concentration of the added N protein is observed (R^2 = 0.9345). The detection of limit (LOD) is calculated as below:

$$\mathrm{LOD} = \frac{3Sa}{b}, \quad (2)$$

where Sa is the standard deviation of the response, and b is the

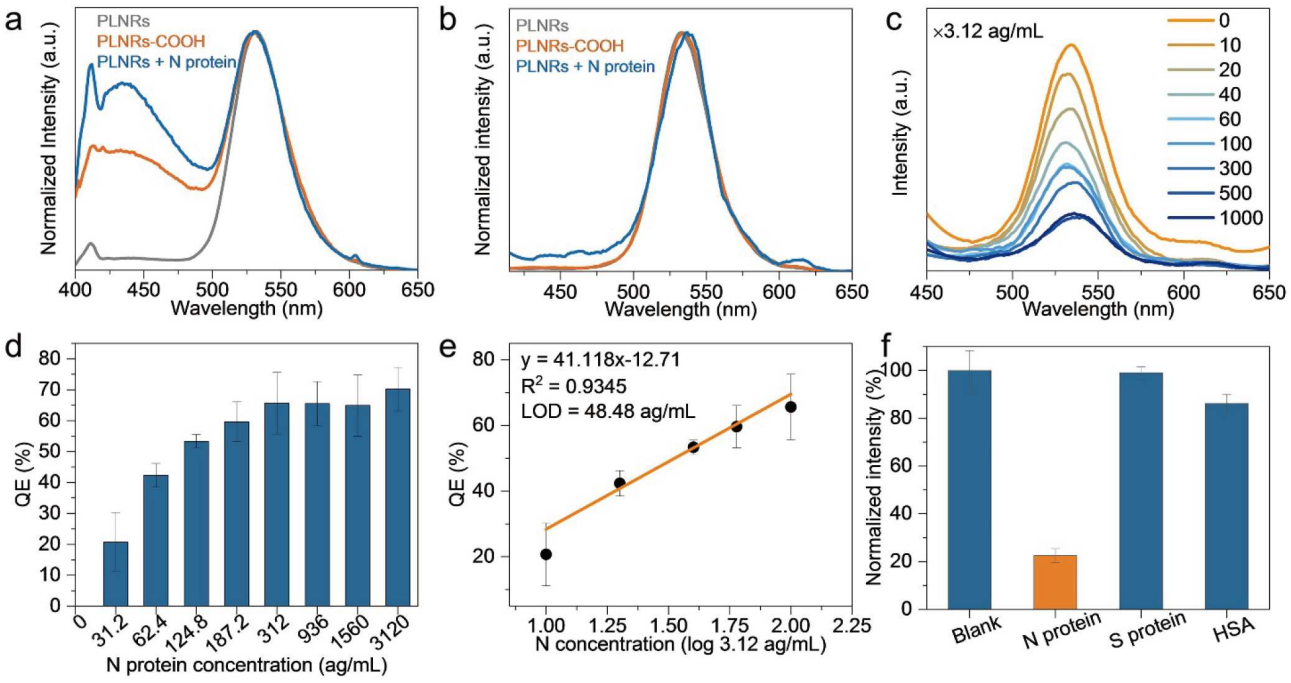

Figure 5 Normalized (a) photoluminescence emission and (b) persistent luminescence spectra of ZGO:Mn,Cr PLNRs, PLNRs-COOH, and PHNRs-antibody1. (c) The persistent luminescence spectra in solution I with the increase of N-protein concentration. The (d) quenching efficiency and (e) corresponding linear fitting for ZGO:Mn,Cr PLNRs. (f) Specificity of the sandwich assay by using N protein, S protein and HSA.

Table 1 The biosensor performance of the recently reported persistent biosensors

Materials	Target	LOD	Range	Ref.
$Ca_{1.86}Mg_{0.14}ZnSi_2O_7:Eu^{2+},Dy^{3+}$	α-Fetoprotein	0.41 μg/mL	0.8–45 μg/mL	[49]
$ZnGa_2O_4:Cr^{3+}$	Glucose	0–500 μM	49.4 μM	[50]
$Zn_2GeO_4:Mn^{2+}$	Aflatoxin B1	0.29 pg/ mL	0.001–50 ng/mL	[51]
$Zn_{1.25}Ga_{1.5}Ge_{0.25}O_4:Cr^{3+},Yb^{3+},Er^{3+}$	Zearalenone	0.22 pg/mL		
$ZnGa_2O_4:Cr^{3+}$	*L*-Cys	2.2 nM	10 nM–5.5 μM	[41]
$ZnGa_2O_4:Cr^{3+}$	MicroRNA21	0.1 nM	0.1–10 nM	[40]
$Zn_2GeO_4:Mn^{2+}$	Ochratoxin A	3 pg/mL	0.01–10 ng/mL	[2]
$Zn_2GeO_4:Mn^{2+}$, Cr^{3+}	N protein	39.82 ag/mL	31.2–3120 ag/mL	This work

slope of the linear fitting curve. Accordingly, the LOD of N protein detection can achieve 48.48 ag/mL, which shows high sensitivity. It is noted that Fe_3O_4 MNPs exhibit strong absorption in the region of 200–800 nm, which largely overlaps with the persistent spectrum of ZGO:Mn,Cr PLNRs (Fig. S5). This result demonstrates that the low LOD value is mainly attributed to the fluorescence resonance energy transfer. To further confirm the repetition of the detection sensitivity, we repeated N protein detection results for several times, the calculated LOD values are in the region of 39.82–119.9 ag/mL (Table S1). The above results confirm the good reproducibility of this detection methods, further confirming the reliable design insight based on ZGO:Mn,Cr PLNRs and Fe_3O_4 MNPs. Additionally, Table 1 exhibits some biosensors based on persistently luminescence materials, demonstrating that our detection method shows significant sensitivity.

Specificity is a paramount specification of the assay. A cross-reaction analysis was executed to evaluate the analytical specificity of our proposed assay. As shown in Fig. 5f and Fig. S6, the specificity detection was performed with N protein, S protein and HSA target samples. The N protein target shows a QE of 73.5%, while spike protein (S protein) and HSA targets shows QE values of around 1% and 13.8%. The above results indicate that the ZGO:Mn,Cr PLNRs and Fe_3O_4 MNPs sandwich-based immunoluminescence assay is highly specific for N protein detection.

A useful and practical assay should be primarily tested with human isolate sample to explore their potential for future applications. The detection of inactivated SARS-CoV-2 virus sample from people saliva was obtained from the Faculty of Medicine, University of Hong Kong. Fig. S7 exhibits persistently luminescence spectra and QE value by using ZGO:Mn,Cr PLNRs and Fe_3O_4 MNPs for the clinical detection of SARS-CoV-2 virus sample. With the addition of SARS-CoV-2 virus sample, the persistent luminescence undoubtedly decreases. Then persistent luminescence intensity gradually decreases with increasing N protein concentration from 0.05 to 1 μL, of which the QE value can be realized as high as 94.5%. The above results indicate that

the fabricated biosensor based on persistent luminescence have promising applications in clinical sample detection. Besides, this strategy can be well extended to the detection of other disease biomarkers by choosing suitable antibodies and antigens. Although the persistent luminescence detection has discernible advantages of autofluorescence-free in the biosensor field, the persistent luminescence stability requires a further calibration for the future practical applications.

CONCLUSIONS

In summary, we design Cr^{3+} co-doping ZGO:Mn PLNRs, whose the persistent luminescence intensity and afterglow time are remarkably enhanced. The underlying persistent luminescence enhancement mechanism is attributed to the generation of deep electron trap via the co-doping of Cr^{3+}. Since the as-prepared ZGO:Mn,Cr samples exhibit bright persistent luminescence for tens of minutes, a biosensor was constructed by combining ZGO:Mn,Cr and Fe_3O_4 MNPs with the corresponding antibody for N protein detection. This biosensor based on persistent luminescence can significantly avoid the autofluorescence in the reaction solution, leading to a low LOD value of 39.82 ag/mL. Meanwhile, the designed biosensors display high specificity and the potential in clinical target detection. Although great progress has been achieved in persistent biosensors, some challenges including persistent luminescence intensity calibration, persistent luminescence stability and the fabrication of biosensors need to be further studied. To conclude, this work provides a general insight in designing biosensors based on persistent luminescence materials.

Received 22 August 2024; accepted 7 October 2024; published online 12 November 2024

1 Huang K, Le N, Wang JS, *et al.* Designing next generation of persistent luminescence: recent advances in uniform persistent luminescence nanoparticles. Adv Mater, 2022, 34: e2107962
2 Jiang YY, Zhao X, Chen LJ, *et al.* Persistent luminescence nanorod based luminescence resonance energy transfer aptasensor for autofluorescence-free detection of mycotoxin. Talanta, 2020, 218: 121101
3 Wang J, Jiang Z, Wei Y, *et al.* Multiplexed identification of bacterial biofilm infections based on machine-learning-aided lanthanide encoding. ACS Nano, 2022, 16: 3300–3310
4 Yang L, Gai S, Ding H, *et al.* Recent progress in inorganic afterglow materials: mechanisms, persistent luminescent properties, modulating methods, and bioimaging applications. Adv Opt Mater, 2023, 11: 2202382
5 Lécuyer T, Seguin J, Balfourier A, *et al.* Fate and biological impact of persistent luminescence nanoparticles after injection in mice: A one-year follow-up. Nanoscale, 2022, 14: 15760–15771
6 Liang L, Chen N, Jia Y, *et al.* Recent progress in engineering near-infrared persistent luminescence nanoprobes for time-resolved biosensing/bioimaging. Nano Res, 2019, 12: 1279–1292
7 Liu N, Shi J, Wang Q, *et al. In vivo* repeatedly activated persistent luminescence nanoparticles by radiopharmaceuticals for long-lasting tumor optical imaging. Small, 2020, 16: e2001494
8 Luo Q, Wang W, Tan J, *et al.* Surface modified persistent luminescence probes for biosensing and bioimaging: a review. Chin J Chem, 2021, 39: 1009–1021
9 Zhao T, Abdurahman R, Aiwaili R, *et al.* Spinel-type persistent luminescence nanoparticles: From mechanisms, compositions to applications. Coord Chem Rev, 2023, 488: 215171
10 Withers PJ, Bouman C, Carmignato S, *et al.* X-ray computed tomography. Nat Rev Methods Primers, 2021, 1: 18
11 Wu L, Li G, Xu X, *et al.* Application of nano-ELISA in food analysis: Recent advances and challenges. TrAC Trends Anal Chem, 2019, 113: 140–156
12 Veith J, Chaigne T, Svanidze A, *et al.* The mechanism for directional hearing in fish. Nature, 2024, 631: 118–124
13 Pontone G, Scafuri S, Mancini ME, *et al.* Role of computed tomography in COVID-19. J Cardiovasc Computed Tomography, 2021, 15: 27–36
14 Song M, Yang M, Hao J. Pathogenic virus detection by optical nanobiosensors. Cell Rep Phys Sci, 2021, 2: 100288
15 Jiang M, Deng Z, Zeng S, *et al.* Recent progress on lanthanide scintillators for soft X-ray-triggered bioimaging and deep-tissue theranostics. VIEW, 2021, 2: 20200122
16 Ma Y, Song M, Li L, *et al.* Advances in upconversion luminescence nanomaterial-based biosensor for virus diagnosis. Exploration, 2022, 2: 20210216
17 Binny RN, Priest P, French NP, *et al.* Sensitivity of reverse transcription polymerase chain reaction tests for severe acute respiratory syndrome coronavirus 2 through time. J Infect Dis, 2022, 227: 9–17
18 Zhao Q, Lu D, Zhang G, *et al.* Recent improvements in enzyme-linked immunosorbent assays based on nanomaterials. Talanta, 2021, 223: 121722
19 Huo Y, Liu S, Gao Z, *et al.* State-of-the-art progress of switch fluorescence biosensors based on metal-organic frameworks and nucleic acids. Microchim Acta, 2021, 188: 168
20 Chai F, Cheng D, Nasu Y, *et al.* Maximizing the performance of protein-based fluorescent biosensors. Biochem Soc Trans, 2023, 51: 1585–1595
21 Ma Y, Song M, Li L, *et al.* Attomolar-level detection of respiratory virus long-chain oligonucleotides based on FRET biosensor with upconversion nanoparticles and Au–Au dimer. Biosens Bioelectron, 2024, 243: 115778
22 Lao X, Liu Y, Li L, *et al.* Plasmon-enhanced FRET biosensor based on Tm^{3+}/Er^{3+} co-doped core-shell upconversion nanoparticles for ultrasensitive virus detection. Aggregate, 2023, 5: e448
23 Li L, Song M, Lao X, *et al.* Rapid and ultrasensitive detection of SARS-CoV-2 spike protein based on upconversion luminescence biosensor for COVID-19 point-of-care diagnostics. Mater Des, 2022, 223: 111263
24 Song M, Ma Y, Li L, *et al.* Multiplexed detection of SARS-CoV-2 based on upconversion luminescence nanoprobe/MXene biosensing platform for COVID-19 point-of-care diagnostics. Mater Des, 2022, 223: 111249
25 Oliveira E, Bértolo E, Núñez C, *et al.* Green and red fluorescent dyes for translational applications in imaging and sensing analytes: a dual-color flag. ChemistryOpen, 2018, 7: 9–52
26 Li C, Liu C, Fan Y, *et al.* Recent development of near-infrared photoacoustic probes based on small-molecule organic dye. RSC Chem Biol, 2021, 2: 743–758
27 Rakovich A, Rakovich T. Semiconductor *versus* graphene quantum dots as fluorescent probes for cancer diagnosis and therapy applications. J Mater Chem B, 2018, 6: 2690–2712
28 Zuo M, Duan Q, Li C, *et al.* A versatile strategy for constructing ratiometric upconversion luminescent probe with sensitized emission of energy acceptor. Anal Chem, 2021, 93: 5635–5643
29 Wu Y, Ali MRK, Chen K, *et al.* Gold nanoparticles in biological optical imaging. Nano Today, 2019, 24: 120–140
30 Meng L, Ma X, Jiang S, *et al.* High-efficiency fluorescent and magnetic multimodal probe for long-term monitoring and deep penetration imaging of tumors. J Mater Chem B, 2019, 7: 5345–5351
31 Zhuang Y, Ueda J, Tanabe S. Photochromism and white long-lasting persistent luminescence in Bi^{3+}-doped $ZnGa_2O_4$ ceramics. Opt Mater Express, 2012, 2: 1378–1383
32 Pan Z, Lu YY, Liu F. Sunlight-activated long-persistent luminescence in the near-infrared from Cr^{3+}-doped zinc gallogermanates. Nat Mater, 2011, 11: 58–63
33 Yoo S, Song Y, Hahn S. Ultralong persistent luminescence from carbon dots. Light Sci Appl, 2022, 11: 132
34 Luo X, Ahn JY, Kim SH. Aerosol synthesis and luminescent properties of $CaAl_2O_4$: Eu^{2+}, Nd^{3+} down-conversion phosphor particles for enhanced light harvesting of dye-sensitized solar cells. Sol Energy, 2019, 178: 173–180

35 Francisco LHC, Moreira RP, Felinto MCFC, *et al.* $SrAl_2O_4$: Eu^{2+}, Dy^{3+} persistent luminescent materials functionalized with the Eu^{3+}(TTA)-complex by microwave-assisted method. J Alloys Compd, 2021, 882: 160608
36 Xue H, Zhu Y, Pang Z, *et al.* Research on a persistent red tone fluorescent polyacrylonitrile fiber with coaxial structure based on $Sr_2MgSi_2O_7$: Eu^{2+}, Dy^{3+} and Y_2O_2S:Eu^{3+}, Mg^{2+}, Ti^{4+}. J Lumin, 2021, 235: 118047
37 Jiang H, Wang R, Zhang Q, *et al.* A dual-functional nanoplatform based on NIR and green dual-emissive persistent luminescence nanoparticles for X-ray excited persistent luminescence imaging and photodynamic therapy. Nanoscale, 2022, 14: 15451–15461
38 Wang J, Ma Q, Zheng W, *et al.* One-dimensional luminous nanorods featuring tunable persistent luminescence for autofluorescence-free biosensing. ACS Nano, 2017, 11: 8185–8191
39 Srivastava BB, Gupta SK, Li Y, *et al.* Bright persistent green emitting water-dispersible Zn_2GeO_4:Mn nanorods. Dalton Trans, 2020, 49: 7328–7340
40 Wang X, Wang Y, Chen S, *et al.* A persistent luminescence resonance energy transfer-based molecular beacon probe for the highly sensitive detection of microRNA in biological samples. Biosens Bioelectron, 2022, 198: 113849
41 Li J, Yang C, Wang WL, *et al.* Functionalized gold and persistent luminescence nanoparticle-based ratiometric absorption and TR-FRET nanoplatform for high-throughput sequential detection of L-cysteine and insulin. Nanoscale, 2018, 10: 14931–14937
42 Liu Y, Yang Y, Wang G, *et al.* Multiplexed discrimination of SARS-CoV-2 variants via plasmonic-enhanced fluorescence in a portable and automated device. Nat Biomed Eng, 2023, 7: 1636–1648
43 Yan L, Chen L, Zhao X, *et al.* pH switchable nanoplatform for *in vivo* persistent luminescence imaging and precise photothermal therapy of bacterial infection. Adv Funct Mater, 2020, 30: 1909042
44 Ji C, Tan J, Yuan Q. Defect luminescence based persistent phosphors—from controlled synthesis to bioapplications. Chin J Chem, 2021, 39: 3188–3198
45 Chen N, Du N, Wang W, *et al.* Real-time monitoring of dynamic microbial Fe(III) respiration metabolism with a living cell-compatible electron-sensing probe. Angew Chem Int Ed, 2022, 61: e202115572
46 Huang K, Dou X, Zhang Y, *et al.* Enhancing Light and X-ray charging in persistent luminescence nanocrystals for orthogonal afterglow anti-counterfeiting. Adv Funct Mater, 2021, 31: 2009920
47 Li J, Huang X, Zhao X, *et al.* pH-responsive torpedo-like persistent luminescence nanoparticles for autofluorescence-free biosensing and high-level information encryption. Angew Chem Int Ed, 2021, 60: 2398–2405
48 Cong Y, He Y, Dong B, *et al.* Long afterglow properties of Zn_2GeO_4: Mn^{2+}, Cr^{3+} phosphor. Optical Mater, 2015, 42: 506–510
49 Wu BY, Wang HF, Chen JT, *et al.* Fluorescence resonance energy transfer inhibition assay for α-fetoprotein excreted during cancer cell growth using functionalized persistent luminescence nanoparticles. J Am Chem Soc, 2011, 133: 686–688
50 Liu J, Viana B, Mignet N, *et al.* H_2O_2-induced persistent luminescence signal enhancement applied to biosensing. Small, 2023, 19: e2303509
51 Jiang YY, Zhao X, Chen LJ, *et al.* A dual-colored persistent luminescence nanosensor for simultaneous and autofluorescence-free determination of aflatoxin B1 and zearalenone. Talanta, 2021, 232: 122395

Acknowledgement The research was supported by a grant from the Research Grants Council of Hong Kong (CRF No. PolyU C5110-20G) and PolyU Grants (G-SB4G, 1-CD4S and 1-CE0H).

Funding note Open Access funding provided by HK-JULAC.

Author contributions Wei Y, Song M and Li L conceived the idea, designed the experiments, and engineered the samples; Ma Y, Lao X and Liu Y performed the experiments; Wei Y wrote the paper with support from Li G and Hao J. All authors contributed to the general discussion.

Conflict of interest The authors declare that they have no conflict of interest.

Supplementary information Supplementary materials are available in the online version of the paper.

Yi Wei obtained her PhD degree in 2023 from China University of Geosciences and was a research assistant at The Hong Kong Polytechnic University from 2022 to 2023. She is currently a postdoc at China University of Geosciences. Her current research focuses on the design and synthesis of inorganic luminescent materials.

Jianhua Hao is a Chair Professor of materials physics and devices and Director of Research Centre for Nanoscience and Nanotechnology, The Hong Kong Polytechnic University. His research interests include metal-ion-doped luminescent materials and devices, and functional thin-films and heterostructures.

用于SARS-CoV-2 N蛋白超灵敏检测的增强型长余辉发光纳米棒

魏忆[1,2], 宋梦麟[1,3], 李丽华[1], 马颖瑾[1], 老欣悦[1], 刘源[1], 李国岗[2], 郝建华[1*]

摘要 长余辉发光纳米材料关闭光源仍能保持发光，由于其能够完全消除自发组织荧光，在生物传感和生物成像领域展示了潜在应用前景. 尽管长余辉发光材料已经取得了较大的进展，但仍缺少具有低检测限和高灵敏度的长余辉检测平台. 基于此，本文开发了具有优异长余辉和超长余辉时间的Zn_2GeO_4:Mn,Cr纳米棒. 通过创建深缺陷，Cr^{3+}的共掺杂明显提高了余辉强度和余辉时间. 将Zn_2GeO_4:Mn,Cr-抗体和Fe_3O_4磁性纳米粒子-抗体构建成生物传感器，用于N蛋白检测. 获得的检测限可低至 39.82 ag/mL，远低于之前报道的长余辉发光生物传感器，这归因于荧光共振能量传递. 此外，构建的长余辉生物传感器还实现了高检测特异性. 因此，所制备的Zn_2GeO_4:Mn,Cr长余辉发光材料可作为生物传感器的候选材料. 该策略为开发具有高灵敏度和特异性的生物传感平台提供了有效的指导.

